Quantum sensing of supersensitivity for the Ohmic quantum reservoir

Qing-Shou Tan [1,*] Wei Wu,[2] Lan Xu,[3] Jing Liu [4] and Le-Man Kuang[5,6,†]

[1]*Key Laboratory of Hunan Province on Information Photonics and Freespace Optical Communication, College of Physics and Electronics, Hunan Institute of Science and Technology, Yueyang 414000, China*
[2]*Key Laboratory of Theoretical Physics of Gansu Province, and Lanzhou Center for Theoretical Physics, Lanzhou University, Lanzhou 730000, China*
[3]*School of Physics and Chemistry, Hunan First Normal University, Changsha 410205, China*
[4]*MOE Key Laboratory of Fundamental Physical Quantities Measurement, National Precise Gravity Measurement Facility, School of Physics, Huazhong University of Science and Technology, Wuhan 430074, China*
[5]*Key Laboratory of Low-Dimensional Quantum Structures and Quantum Control of Ministry of Education, Department of Physics and Synergetic Innovation Center for Quantum Effects and Applications, Hunan Normal University, Changsha 410081, China*
[6]*Synergetic Innovation Academy for Quantum Science and Technology, Zhengzhou University of Light Industry, Zhengzhou 450002, China*

We propose an approach to implement a supersensitive estimation of the key parameters of the Ohmic-family spectral density with coherent spin states as the quantum sensor. This method can dramatically improve the estimation precision of the reservoir coupling strength as well as the cutoff frequency of the spectral density, by using both the number of spins N and encoding time t as effective resources. The quantum Fisher information indicates that the estimation sensitivity of the spectral density can surpass the shot-noise limit for all the sub-Ohmic, Ohmic, and super-Ohmic reservoirs. In particular, for super-Ohmic reservoirs, the precision can achieve a scaling $\propto 1/(Nt)$. We also present the measurement scheme which can saturate the quantum Cramér-Rao bound.

I. INTRODUCTION

Quantum systems inevitably interact with an environment that causes the loss of quantum coherence, called quantum decoherence [1]. Understanding and preventing decoherence is at the center of the field of quantum information [2]. In fact, many quantum optimal control protocols [3–7], which are used to suppress decoherence, require as much information as possible about the environment. A complex quantum reservoir can be characterized by a spectral density function which determines how and how fast a quantum system loses coherence. The key parameters of spectral density are not directly observable, and hence detecting a spectral density will play a vital role in controlling the reservoir causing decoherence to quantum systems. Recently, many schemes have been proposed to measure the spectral density [8–16].

Quantum sensing of an environment aims at extracting precise information about the environment [17–19], such as the spectral density, via the interaction of a simple quantum system with the environment. This topic has a natural connection with the theory of quantum metrology [20–24], where the aim is to attain a precision that surpasses the shot-noise limit (SNL) by using quantum resources. According to the protocol of quantum metrology [25], one of the most important steps is parametrization, where usually the parameter to be estimated is encoded into the probe's state by a unitary rotation. How-

ever, to sense a spectral density via coupling the sensor with a reservoir will make the dynamics of the sensor nonunitary. This nonunitary-encoding quantum sensing scheme in turn degrades the quantum resources of the sensors and will encounter a so-called error-divergency problem [12–14], which makes the sensing precision to the spectral density worse and worse with increased encoding time. Reference [15] reported that the initial correlations between the sensor and the environment can improve the precision when sensing sub-Ohmic reservoirs. Reference [16] found that a bound-state mechanism can efficiently eliminate the error-divergence problem of sensing quantum reservoirs, and showed that the precision can reach a scaling $\propto 1/t$ in the long encoding time regime. There, the encoding time t is recovered as a resource to enhance the precision of the sensing of a quantum reservoir. However, previous works [12–16] concerning the estimation of bosonic spectral density parameters have only focused on single- or two-qubit probes. A natural question is whether the precision can be further improved by using the qubit ensemble as the sensor. Can both the number of qubits N and encoding time t be used as resources to improve the estimation accuracy?

In this paper, we propose a supersensitive sensing scheme for the spectral density of a quantum reservoir by using an N two-level system as the quantum sensor. We find that the information of the spectral density is written in the sensor's quantum state through both unitary encoding and nonunitary encoding: a reservoir-induced nonlinear interaction and decoherence function. The nonlinear interaction can dramatically improve the estimation precision of the quantum reservoir. Especially, in the super-Ohmic regime, the decoherence

*qstan@hnist.edu.cn
†lmkuang@hunnu.edu.cn

effect of the reservoir will be significantly suppressed, then the unitary encoding will play a leading role. By calculating the quantum Fisher information (QFI) [26,27], a key quantity in quantum metrology, we find that for a super-Ohmic reservoir the sensing sensitivity of the spectral density can reach a scaling $\propto 1/(Nt)$. It indicates that both the number of spins N and encoding time t can be used as resources to enhance the estimation accuracy of a quantum reservoir when using coherent spin states (CSSs) as the quantum sensor.

II. QUANTUM PARAMETER ESTIMATION AND QUANTUM FISHER INFORMATION

In quantum metrology, the estimation precision for an unknown parameter X can be characterized by the quantum Cramér-Rao bound

$$\Delta X \geqslant 1/\sqrt{\nu \mathcal{F}_X}, \tag{1}$$

which gives a theoretically achievable limit on the precision. Here, ν is the number of independent measurements (we set $\nu = 1$), and the QFI $\mathcal{F}_X$, with respect to X, is defined by $\mathcal{F}_X = \text{Tr}[\rho_X L_X^2]$, in which ρ_X is the quantum states depending on the parameter X, and L_X is the so-called symmetric logarithmic derivative determined by the equation $\partial \rho_X/\partial X = [\rho_X L_X + L_X \rho_X]/2$. Physically, the QFI also can be expressed in terms of the Uhlmann fidelity $f(\rho_1, \rho_2) = (\text{Tr}\sqrt{\sqrt{\rho_1}\rho_2\sqrt{\rho_1}})^2$ via the relation [28,29]

$$\mathcal{F}_X = \lim_{\epsilon \to 0} \frac{8(1 - \sqrt{f[\rho_X(t), \rho_{X+\epsilon}(t)]})}{\epsilon^2}, \tag{2}$$

which unveils the distinguishability between two infinitesimally distant quantum states. Based on the quantum Cramér-Rao bound, a large QFI means a high precision of the estimation. It is equivalent to enhancing the ability of distinguishing between neighboring states, depending on X, and reducing the error associated with the estimation procedure. Thus increasing the QFI is important in enhancing the precision of the parameter estimation. In general, QFI improves with an increasing number of probes (N) or the encoding time (t) employed in the measurement. For classical strategies, optimal QFI scales as N, called SNL. By exploiting the quantum resources, the QFI can achieve N^2 scaling. This is known as Heisenberg scaling. In what follows we will utilize a spin ensemble as a probe to obtain N^2 scaling in a number of spins and t^2 scaling in the encoding time, for sensing the quantum reservoir. That is, $\Delta X \propto 1/(Nt)$ [30], in which both N and t are used as resources to improve the precision.

III. QUANTUM SENSING TO THE QUANTUM RESERVOIR

We now consider the case of N spins, acting as the quantum sensor, coupled to a common reservoir with a dephasing interaction. We employ the sensor to estimate the parameters of a bosonic reservoir, and the total Hamiltonian of the sensor plus the quantum reservoir is described as [1]

$$H = \omega_s J_z + \sum_k \omega_k a_k^\dagger a_k + \sum_k J_z(g_k a_k^\dagger + g_k^* a_k), \tag{3}$$

where ω_s is the frequency of the sensor system, and $J_z = \sum_{i=1}^N \frac{1}{2}\sigma_z^{(i)}$ is the collective angular momentum operator with

N the number of spins and $\sigma_z^{(i)}$ the Pauli matrix for the ith spin. $a_k^\dagger$ (a_k) denotes the bosonic creation (annihilation) operator for mode k, ω_k is the frequency of the kth mode, and g_k is the corresponding coupling constant with the qubits. The couplings g_k are distributed according to different spectral distributions of the reservoir, and hence lead to different dynamical properties for the qubits. The effect of the reservoir on the system is encapsulated by the spectral density $J(\omega) \equiv \sum_k |g_k|^2 \delta(\omega - \omega_k)$ in the continuum limit of the frequency.

In this paper we will consider Ohmic-family spectral densities of the form

$$J(\omega) = \eta \omega^s \omega_c^{1-s} e^{-\omega/\omega_c}, \tag{4}$$

where η is the coupling (damping) strength of reservoir, and ω_c is the cutoff frequency which characterizes the correlation timescale of the reservoir. Both η and ω_c are important parameters of the spectral density that we want to estimate. The value of s classifies the nature of the reservoir, often referred to as sub-Ohmic when $0 < s < 1$, Ohmic when $s = 1$, and super-Ohmic when $s > 1$. The Ohmic-family spectral densities are proper choices for a spin-boson model [31]. For instance, Ohmic spectral density was widely considered for electron transfer dynamics [32] or biomolecular complexes [33], as well as Josephson junctions [34]. When charge qubits are subjected to a phonon bath, super-Ohmic spectral density may be a good choice [35]. Moreover, when an impurity qubit is immersed in a dipolar Bose-Einstein condensate, the properties of the environment (collective excitations) can be engineered from sub-Ohmic to super-Ohmic spectral density by tuning the relative strength of the dipolar and contact interactions [36].

Taking the interaction picture with respect to the reservoir operator $\sum_k \omega_k a_k^\dagger a_k \to \int_0^\infty d\omega a_\omega^\dagger a_\omega$ in the continuum limit of the frequency, the time evolution operator can be obtained by using the Magnus expansion [37–40] (see the Appendix for details)

$$U(t) = \exp\left\{-i[\omega_s t J_z + \Delta(t)J_z^2]\right\} V(t). \tag{5}$$

The noise-induced nonlinear interaction strengthens $\Delta(t) = \int_0^\infty d\omega J(\omega)\frac{\omega t - \sin(\omega t)}{\omega^2}$, which carries all the message on $J(\omega)$, and can be obtained as

$$\Delta(t) = \begin{cases} \eta\Gamma(s)[\omega_c t - (1 + t^2\omega_c^2)^{-s/2}\Phi(s,t)], & s \neq 1, \\ \eta[\omega_c t - \arctan(\omega_c t)], & s = 1, \end{cases} \tag{6}$$

where

$$\Phi(s,t) = \frac{\sin[s\arctan(\omega_c t)] - \omega_c t \cos[s\arctan(\omega_c t)]}{s-1}$$

and $\Gamma(s)$ is the Euler gamma function defined as $\Gamma(s) = \int_0^\infty e^{-x}x^{s-1}dx$.

In Eq. (3), the interaction term between the sensor and reservoir reads

$$V(t) = \exp\left\{J_z \int_0^\infty d\omega[\alpha_\omega(t)a_\omega^\dagger - \alpha_\omega^*(t)a_\omega]\right\}, \tag{7}$$

with $\alpha_\omega(t) = \sqrt{J(\omega)}(1 - e^{i\omega t})/\omega$, which determines the nonunitary dynamics of the system.

At time $t = 0$, the sensor and reservoir are assumed to be in a factorized state

$$\rho(0) = |\Psi(0)\rangle\langle\Psi(0)| \otimes \rho_B. \tag{8}$$

Here, $|\Psi(0)\rangle = |\theta, \phi\rangle$ is the coherent spin state (CSS)

$$|\theta, \phi\rangle = \sum_{m=-J}^{m=J} c_m |J, m\rangle, \tag{9}$$

with $J = N/2$ being the total spin, and the probability amplitudes are given by

$$c_m = \binom{2J}{J+m}^{\frac{1}{2}} \cos^{J+m}\left(\frac{\theta}{2}\right) \sin^{J-m}\left(\frac{\theta}{2}\right) e^{i(J-m)\phi},$$

in which θ and ϕ are the polar and azimuth angles, respectively. The thermal equilibrium state ρ_B of the reservoir is defined by

$$\rho_B = \bigotimes_\omega [1 - \exp(-\beta\omega)] \exp(-\beta\omega a_\omega^\dagger a_\omega), \tag{10}$$

with $\beta = 1/(k_B T)$ being the inverse temperature.

Then, the exact matrix elements of the sensor's density matrix can be determined from the relation

$$\rho_{m,n}(t) = \text{Tr}_B[\langle J, m|U(t)\rho(0)U^{-1}(t)|J, n\rangle]$$
$$= e^{-i\varphi(t)} e^{-i(m^2-n^2)\Delta(t)} e^{-(m-n)^2 R(t)} \rho_{m,n}(0), \tag{11}$$

with $\varphi(t) = (m - n)\omega_s t$ and $\rho_{m,n}(0) = c_m c_n^*$. Here, $R(t)$ is the decoherence function which also depends upon the spectral density of the reservoir,

$$R(t) = \int_0^\infty J(\omega) \coth\left(\frac{\beta\omega}{2}\right) \frac{1 - \cos(\omega t)}{\omega t}. \tag{12}$$

For a zero-temperature environment ($T = 0$), the explicit expression of the decoherent function can be obtained as [41,42]

$$R(t) = \begin{cases} \eta\Gamma(s-1)\left\{1 - \frac{\cos[(s-1)\arctan(\omega_c t)]}{(1+\omega_c^2 t^2)^{(s-1)/2}}\right\}, & s \neq 1, \\ \frac{\eta}{2} \ln[(1 + \omega_c^2 t^2)], & s = 1. \end{cases} \tag{13}$$

Based on Eq. (11), we can find that the message of $J(\omega)$ is written into the sensor's density matrix by both $\Delta(t)$ (unitary encoding) and $R(t)$ (nonunitary encoding). To clearly see how $\Delta(t)$ and $R(t)$ affect the quantum state of the sensor for different quantum reservoirs, in Fig. 1 we plot both $\Delta(t)$ and $R(t)$ as a function of $\omega_s t$ for various Ohmicity parameters s. It is shown that the noise-induced nonlinear term $\Delta(t) \approx \eta\Gamma(s)\omega_c t$ for all the values of s, which is consistent with Eq. (6). As it is seen in Fig. 1(b), when $s \leqslant 1$ the decoherence function $R(t)$ will tend to be infinite in the long-time limit. While the case is completely different for the super-Ohmic reservoir ($s > 1$), it will tend to a constant value $R(\infty) \to \eta\Gamma(s-1)$. Hence we can conclude that the decoherence effect of the reservoir can be effectively suppressed for super-Ohmic spectral density.

Below, we will calculate the QFIs for ω_c and η of the spectral density based on the encoded quantum state in Eq. (11). Generally, for many-body open systems, the analytical expression of QFIs are very hard to get. With the help of Eq. (2), we can present numerical simulations of the behavior for QFIs with ω_c and η, respectively, for various s and N. Numerically, it is convenient to introduce the following dimensionless
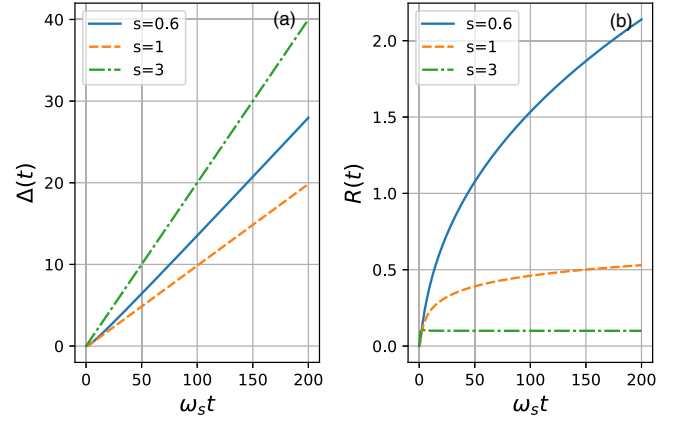

FIG. 1. The functions $\Delta(t)$ and $R(t)$ evolve with dimensionless time $\omega_s t$ for various Ohmicity parameters s. Other dimensionless parameters are chosen as $\eta = 0.1\omega_s$, $\omega_c = \omega_s$, and $T = 0$.

units: $\hbar\omega_s$ for energy, ω_s^{-1} for time, and we set $\hbar = k_B = 1$ throughout this paper.

To demonstrate more clearly the sensing supersensitivity of the parameters of the spectral density, we introduce the ratio of QFIs to $(Nt)^2$, read as $\mathcal{F}_X/(Nt)^2$ with $X = \{\eta, \omega_c\}$. In Fig. 2, we present the dynamical behaviors of the ratios of $\mathcal{F}_\eta/(Nt)^2$ and $\mathcal{F}_{\omega_c}/(Nt)^2$ for all the cases of sub-Ohmic ($s < 1$), Ohmic ($s = 1$), and super-Ohmic ($s > 1$) reservoirs with different N. From Fig. 2, we can see that in both the sub-Ohmic and Ohmic regimes the ratios $\mathcal{F}_X/(Nt)^2$ show a downward trend after reaching the maximum values, as the same as the error-divergency problem for a single-qubit case, while we can still obtain a precision that surpasses the SNL, since there is the trade-off between unitary encoding and nonunitary encoding for the spectral density. However, in the super-Ohmic regime we can clearly see that the ratios tend to constant values depending on N, which means that we can obtain the Heisenberg scaling, for sensing the parameters ω_c and η, and both N and t can be viewed as resources to improve the precision.

Next, we will focus on the analysis of the Heisenberg scaling precision of the sensing for a quantum reservoir in the super-Ohmic regime. Recalling Fig. 1, we know when $s > 1$ the decoherence function $R(t)$ will tend to a constant value $\eta\Gamma(s-1)$ in the long-time limit. Particularly, in the weak-coupling limit $\eta/\omega_s \ll 1$, we may have $R \to 0$ when $s > 1$. Thus, the unitary-encoding scheme plays a major role in the super-Ohmic spectral regime, that is,

$$U_{X=\{\omega_c, \eta\}} \approx \exp\left[-it\Gamma(s)\eta\omega_c J_z^2\right]. \tag{14}$$

As reported in Ref. [43], this is second-order nonlinearity in J_z and a sensitivity limit of $\Delta(\eta\omega_c t) \propto N^{-3/2}$ can be achieved even in the absence of entanglement, called "super-Heisenberg" scaling [23,44,45]. Therefore, for $X = \{\eta, \omega_c\}$, the QFIs $\mathcal{F}_X \propto 4[\langle J_z^4\rangle - (\langle J_z^2\rangle)^2]$ can be calculated analytically as follows,

$$\mathcal{F}_\eta \approx \omega_c^2\Gamma^2(s)t^2\mathcal{Q}, \quad \mathcal{F}_{\omega_c} \approx \eta^2\Gamma^2(s)t^2\mathcal{Q}, \tag{15}$$

where

$$\mathcal{Q} = \frac{N(2N-3)(N-1)}{8}\sin^2(2\theta) + \frac{N(N-1)}{2}\sin^2\theta.$$
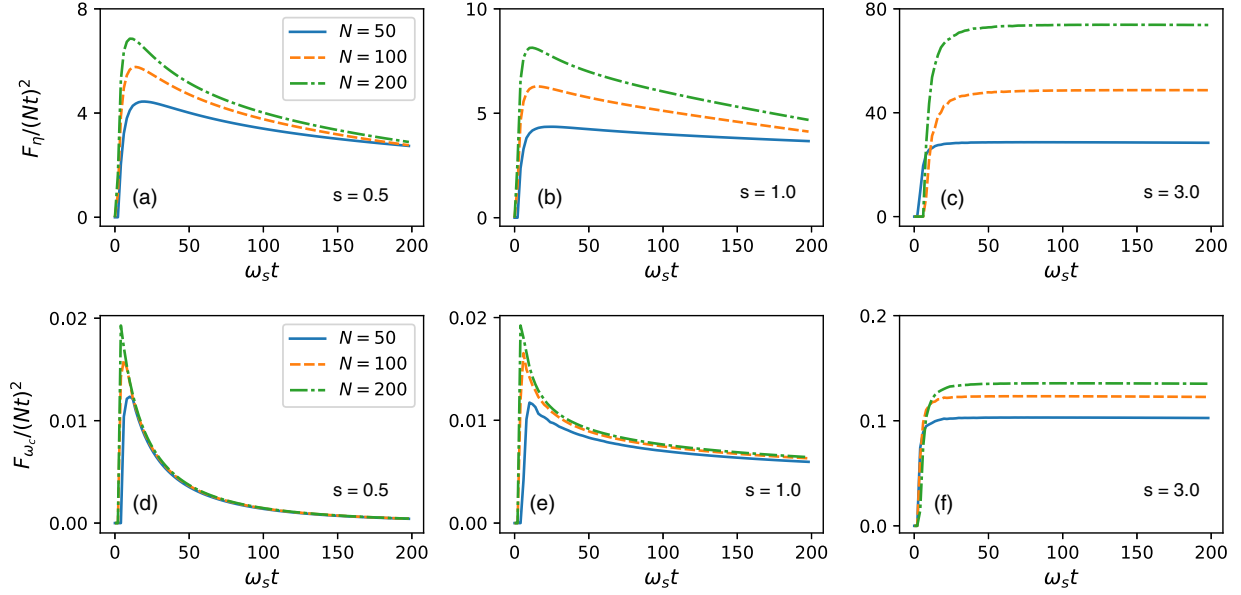
FIG. 2. (a)–(c) plot the behaviors of $\mathcal{F}_\eta/(Nt)^2$ as a function of the dimensionless time $\omega_s t$ for various s and N with $\eta = 0.01\omega_s$ and $\omega_c = \omega_s$. (d)–(f) plot the behaviors of $\mathcal{F}_{\omega_c}/(Nt)^2$ as a function of the dimensionless time $\omega_s t$ for various s and N with $\eta = 0.1\omega_s$ and $\omega_c = \omega_s$. Here, we choose $T = 0$ and $\theta = \pi/6$.

Note that the QFIs $\mathcal{F}_X$ depend on θ but not ϕ, thus without a special statement, we shall choose $\phi = 0$ throughout our discussions. In terms of Eq. (15), then the QFIs can be expressed as $\mathcal{F}_X = k(N, s, \omega_c, \eta, \theta)(Nt)^2$, and the optimal values $\mathcal{F}_X^*$ can be achieved when $\theta^* \approx \pi/4$. It is further verified that the Heisenberg scaling precision can be obtained in the super-Ohmic spectral regime.

However, as can be predicted, with increasing η, i.e., $\eta/\omega_s > 0.01$, the analytical results given in Eq. (15) will be invalid. To illustrate that the Heisenberg scaling precision is still the same for large η, in Figs. 3(a) and 3(b) the optimal ratios $\mathcal{F}_\eta^*/(Nt)^2$ and $\mathcal{F}_{\omega_c}^*/(Nt)^2$ are presented, respectively, as a function of η for $s = 3$ (as an example). As they are shown, we can see that the values of $\mathcal{F}_\eta^*/(Nt)^2$ degrade with an increase of η, because of the decoherence effect. The maximum ratio can be obtained $\mathcal{F}_\eta^*/(Nt)^2 \rightarrow \omega_c^2 \Gamma(s)^2 N/4$ when $\eta \rightarrow 0$, while $\mathcal{F}_{\omega_c}^*/(Nt)^2$ shows the opposite trend, that moderately large η can improve the QFI. In both cases, large N can help to improve the ratios $\mathcal{F}_X/(Nt)^2$. In Fig. 3(c), we also show the corresponding optimal polar angles θ^* of the initial CSS

as a function of η, where we can see that the optimal polar angles θ^* depend on both η and N, that is, θ^* decreases with increasing η and N. When $\eta \rightarrow 0$, we have $\theta^* \approx \pi/4$, which is consistent with Eq. (15).

IV. MEASUREMENT

In practical experiments, finding the optimal measurement that can lead to the highest precision of the estimated parameter is of practical importance. Here, we choose the observable $\langle J_x \rangle$ as the measurement signal with $J_x = 1/2 \sum_{i=1}^{N} \sigma_x^{(i)}$ and $\sigma_x^{(i)}$ being the Pauli matrix, and the estimation fluctuation is ΔJ_x^2. Based on the error propagation formula, the minimum standard deviation for an unknown parameter $X = \{\eta, \omega_c\}$ is given by

$$\Delta X = \frac{\Delta J_x}{|\partial \langle J_x \rangle / \partial X|}. \tag{16}$$
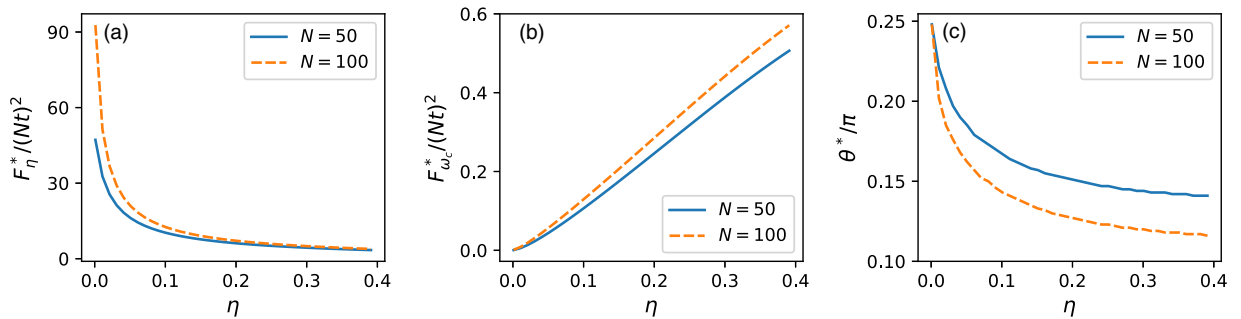

FIG. 3. (a) and (b) plot the optimal QFIs $\mathcal{F}_\eta^*/(Nt)^2$ and $\mathcal{F}_{\omega_c}^*/(Nt)^2$ as a function of dimensionless coupling strength η with particle numbers $N = 50$ and 100, respectively. (c) The optimal polar angle θ^* of the initial CSS as a function of dimensionless coupling strength η with particle numbers $N = 50$ and 100. Here, we choose $T = 0$, $\omega_c = \omega_s$, $\omega_s t = 100$, and $s = 3$ corresponding to the super-Ohmic reservoir.
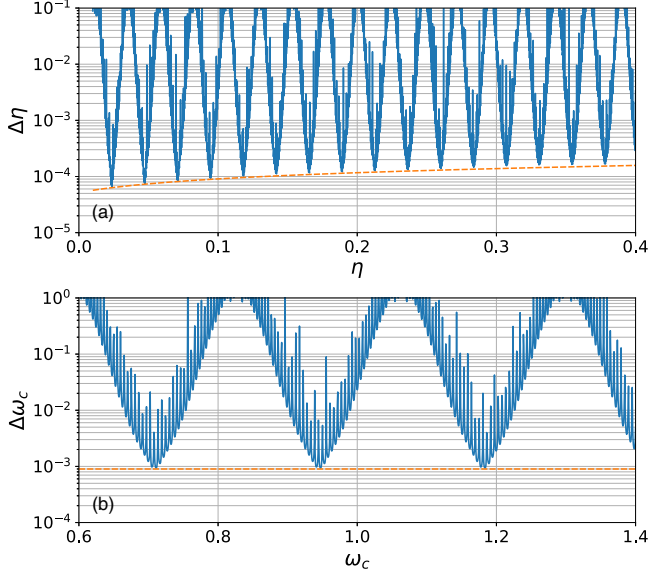
FIG. 4. (a) The precision $\Delta\eta$ on the dimensionless parameter η with $\omega_c = \omega_s$. (b) The precision $\Delta\omega_c$ on the dimensionless parameter ω_c with $\eta = 0.1\omega_s$. The solid lines (blue) and the dotted lines (orange), respectively, correspond to the precisions given by Eq. (16) and the quantum Cramér-Rao bound $\Delta X_{\mathrm{QCR}} = 1/\sqrt{\mathcal{F}_X}$ with $X = \{\eta, \omega_c\}$. Here, other parameters are chosen as follows: $N = 50$, $T = 0$, $\omega_s t = 100$, $\theta = \pi/6$, $\phi = 0$, and $s = 2.5$.

The variance ΔJ_x^2 and the mean value $\langle J_x \rangle$, respectively, read as [46]

$$\Delta J_x^2 = \frac{1}{2}\{J(J - 1/2)\sin^2(\theta) + J + \mathrm{Re}[\langle J_+^2 \rangle]\} - \langle J_x \rangle^2,$$
$$\langle J_x \rangle = \mathrm{Re}[\langle J_+ \rangle], \tag{17}$$

where $\mathrm{Re}[\mathcal{C}]$ represents the real part of $\mathcal{C}$, and

$$\langle J_+ \rangle = e^{i(\omega_s t + \phi)} e^{-R(t)} J \sin(\theta)$$
$$\times \{\cos[\Delta(t)] - i\cos(\theta)\sin[\Delta(t)]\}^{2J-1}, \tag{18}$$

$$\langle J_+^2 \rangle = e^{2i(\omega_s t + \phi)} e^{-4R(t)} J(J - 1/2)\sin^2(\theta)$$
$$\times \{\cos[2\Delta(t)] - i\cos(\theta)\sin[2\Delta(t)]\}^{2J-2}. \tag{19}$$

After some calculations, we can get $|\partial\langle J_x \rangle/\partial X|$, which reflects the sensitivity of the measurement signal to parameter X. For the super-Ohmic spectral density, when $\omega_c t \gg 1$, we have

$$\frac{\partial\langle J_x \rangle}{\partial\eta} \approx \mathrm{Re}\{[\omega_c t\Gamma(s)(2J - 1)\Theta(s, \theta, t) - \Gamma(s - 1)]\langle J_+ \rangle\},$$

$$\frac{\partial\langle J_x \rangle}{\partial\omega_c} \approx \eta t\Gamma(s)(2J - 1)\mathrm{Re}[\langle J_+ \rangle\Theta(s, \theta, t)] \tag{20}$$

with

$$\Theta(s, \theta, t) = -\frac{\sin[\eta\Gamma(s)t\omega_c] + i\cos(\theta)\cos[\eta\Gamma(s)t\omega_c]}{\cos[\eta\Gamma(s)t\omega_c] - i\cos(\theta)\sin[\eta\Gamma(s)t\omega_c]}.$$

Then, following the error propagation formula given in Eq. (16), we can directly obtain the estimation precisions of $\Delta\omega_c$ and $\Delta\eta$.

In Fig. 4, we plot the estimation precisions of the coupling strength $\Delta\eta$ and cutoff frequency $\Delta\omega_c$ as functions of η and ω_c, respectively. Here, we choose $s = 2.5$ as an example of super-Ohmic spectral density and $N = 50$, $\omega_s t = 100$. As shown in Fig. 4, we find that the accuracy of $\Delta\eta$ and $\Delta\omega_c$ can be in accordance with the best precisions given by the Cramér-Rao bound at some optimal points. This means that both the precisions of $\Delta\eta$ and $\Delta\omega_c$ can achieve a scaling $\propto 1/(Nt)$.

V. CONCLUSION

In summary, we have presented a scheme to attain supersensitive quantum sensing for the spectral density of a quantum reservoir by using uncorrelated CSS as the quantum sensor. We discovered that the information of the spectral density can be encoded into the sensor's quantum state via two different mechanisms. In addition to nonunitary encoding, there is also a unitary encoding. Through calculating the QFIs of the sensor, we found that the unitary-encoding mechanism can remarkably improve the estimation precision of both the sensor-reservoir coupling strength and the cutoff frequency of the Ohmic-family spectral density. Compared with the case of sub-Ohmic and Ohmic spectral densities, for the super-Ohmic case the estimation precision can achieve $1/N$ scaling in a number of spins and $1/t$ scaling in the encoding time. It indicates that both the number of spins and encoding time can be used as resources to enhance the estimation accuracy of a quantum reservoir, owing to the decoherence effect of the reservoir being greatly suppressed and the unitary encoding playing a leading role. Furthermore, we have demonstrated that the superprecision given by the QCR bound can be realized by implementing the measurement of the collective angular momentum operator J_x on the sensor. Our studies pave a way to realize high-precision sensing of a quantum reservoir by utilizing a spin ensemble as a probe, and the results can be also helpful for the estimation of environmental noise parameters in other settings such as quantum noise spectroscopy.

APPENDIX: DERIVATION OF THE TIME EVOLUTION OPERATOR $U(t)$

In this Appendix, we present a detailed derivation of Eq. (5). First, we substitute the spectral density into Eq. (3) in the continuum limit of the frequency. After taking the interaction picture with respect to $\int_0^\infty d\omega a_\omega^\dagger a_\omega$, the Hamiltonian H then becomes [14]

$$H'(t) = \omega_s J_z + J_z \int_0^\infty d\omega \sqrt{J(\omega)}(a_\omega e^{-i\omega t} + a_\omega^\dagger e^{i\omega t}), \tag{A1}$$

by using the commutation relation $[a_\omega, a_{\omega'}^\dagger] = \delta(\omega - \omega')$. The time evolution operator associated with $H'(t)$ can be obtained by using the Magnus expansion as [37]

$$U(t) = T_+ \exp\left[-i\int_0^t H(t')dt'\right] = \exp\left[\sum_{n=1}^\infty \frac{(-i)^n}{n!} F_n(t)\right], \tag{A2}$$

where T_+ is the time-ordering operator, and $F_n(t)$ are given as

$$F_1(t) = \int_0^t H'(t_1)dt_1,$$

$$F_2(t) = \int_0^t dt_1 \int_0^{t_1} dt_2 [H'(t_1), H'(t_2)],$$

$$F_3(t) = \int_0^t dt_1 \int_0^{t_1} dt_2 \int_0^{t_2} dt_3 ([H'(t_1), [H'(t_2), H'(t_3)]] + [H'(t_3), [H'(t_2), H'(t_1)]]),$$

$$\cdots . \tag{A3}$$

Since the commutator $[H'(s), H'(s')] = -2iJ_z^2 \sin[\omega(s-s')]$ commutes with $H'(t)$, therefore in our case only the first two terms of $F_n(t)$ are nonzero,

$$F_1(t) = \omega_s t J_z + J_z \int_0^\infty d\omega [\alpha_\omega(t)a_\omega^\dagger - \alpha_\omega^*(t)a_\omega], \tag{A4}$$

$$F_2(t) = -2iJ_z^2 \int_0^\infty J(\omega)\frac{\omega t - \sin(\omega t)}{\omega^2}, \tag{A5}$$

with $\alpha_\omega(t) = \sqrt{J(\omega)}(1 - e^{-i\omega t})/\omega$. Then the time evolution operator can be obtained as

$$U(t) = \exp\left[-iF_1(t) - \frac{F_2(t)}{2}\right] = \exp\left\{-i[\omega_s t J_z + \Delta(t)J_z^2]\right\}V(t), \tag{A6}$$

with $\Delta(t) = \int_0^\infty J(\omega)\frac{\omega t - \sin(\omega t)}{\omega^2}$ and $V(t) = \exp\{J_z \int_0^\infty d\omega [\alpha_\omega(t)a_\omega^\dagger - \alpha_\omega^*(t)a_\omega]\}$, which corresponds to Eqs. (6) and (7) in the main text. Then, Eq. (5) in the main text is obtained.

[1] H.-P. Breuer and F. Petruccione, *The Theory of Open Quantum Systems* (Oxford University Press, Oxford, U.K., 2002).

[2] M. A. Nielsen and I. L. Chuang, *Quantum Computation and Quantum Information* (Cambridge University Press, Cambridge, UK, 2000).

[3] L. Viola, E. Knill, and S. Lloyd, Dynamical Decoupling of Open Quantum Systems, Phys. Rev. Lett. **82**, 2417 (1999).

[4] A. G. Kofman and G. Kurizki, Universal Dynamical Control of Quantum Mechanical Decay: Modulation of the Coupling to the Continuum, Phys. Rev. Lett. **87**, 270405 (2001).

[5] F. Mascherpa, A. Smirne, S. F. Huelga, and M. B. Plenio, Open Systems with Error Bounds: Spin-Boson Model with Spectral Density Variations, Phys. Rev. Lett. **118**, 100401 (2017).

[6] F. F. Floether, P. de Fouquieres, and S. G. Schirmer, Robust quantum gates for open systems via optimal control: Markovian versus non-Markovian dynamics, New J. Phys. **14**, 073023 (2012).

[7] Q. S. Tan, Y. Huang, X. Yin, L. M. Kuang, and X. Wang, Enhancement of parameter-estimation precision in noisy sys-

tems by dynamical decoupling pulses, Phys. Rev. A **87**, 032102 (2013).

[8] C. Benedetti, F. Buscemi, P. Bordone, and M. G. A. Paris, Quantum probes for the spectral properties of a classical environment, Phys. Rev. A **89**, 032114 (2014).

[9] M. Bina, F. Grasselli, and M. G. A. Paris, Continuous-variable quantum probes for structured environments, Phys. Rev. A **97**, 012125 (2018).

[10] D. Goldwater, P. F. Barker, A. Bassi, and S. Donadi, Quantum Spectrometry for Arbitrary Noise, Phys. Rev. Lett. **123**, 230801 (2019).

[11] D. Farfurnik and N. Bar-Gill, Characterizing spin-bath parameters using conventional and time-asymmetric Hahn-echo sequences, Phys. Rev. B **101**, 104306 (2020).

[12] C. Benedetti, F. S. Sehdaran, M. H. Zandi, and M. G. A. Paris, Quantum probes for the cutoff frequency of Ohmic environments, Phys. Rev. A **97**, 012126 (2018).

[13] F. S. Sehdaran, M. H. Zandi, and A. Bahrampour, The effect of probe-ohmic environment coupling type and probe information

flow on quantum probing of the cutoff frequency, Phys. Lett. A **383**, 126006 (2019).

[14] D. Tamascelli, C. Benedetti, H.-P. Breuer, and M. G. A. Paris, Quantum probing beyond pure dephasing, New J. Phys. **22**, 083027 (2020).

[15] H. Ather and A. Z. Chaudhry, Improving the estimation of environment parameters via initial probe-environment correlations, Phys. Rev. A **104**, 012211 (2021).

[16] W. Wu, S.-Y. Bai, and J.-H. An, Non-Markovian sensing of a quantum reservoir, Phys. Rev. A **103**, L010601 (2021).

[17] C. L. Degen, F. Reinhard, and P. Cappellaro, Quantum sensing, Rev. Mod. Phys. **89**, 035002 (2017).

[18] S. Pirandola, B. R. Bardhan, T. Gehring, C. Weedbrook, and S. Lloyd, Advances in photonic quantum sensing, Nat. Photonics **12**, 724 (2018).

[19] S. Zaiser, T. Rendler, I. Jakobi *et al.*, Enhancing quantum sensing sensitivity by a quantum memory, Nat. Commun. **7**, 12279 (2016).

[20] V. Giovannetti, S. Lloyd, and L. Maccone, Quantum Metrology, Phys. Rev. Lett. **96**, 010401 (2006).

[21] V. Giovannetti, S. Lloyd, and L. Maccone, Advances in quantum metrology, Nat. Photonics **5**, 222 (2011).

[22] J. Ma, X. G. Wang, C. P. Sun, and N. Franco, Spin squeezing, Phys. Rep. **509**, 89 (2011).

[23] Z. Hou, Y. Jin, H. Chen, J. F. Tang, C. J. Huang, H. Yuan, G. Y. Xiang, C. F. Li, and G. C. Guo, Super-Heisenberg and Heisenberg Scalings Achieved Simultaneously in the Estimation of a Rotating Field, Phys. Rev. Lett. **126**, 070503 (2021).

[24] J. Liu, M. Zhang, H. Chen, L. Wang, and H. Yuan, Optimal scheme for quantum metrology, Adv. Quantum Technol. **5**, 2100080 (2022).

[25] J. Liu, H. Yuan, X. M. Lu, and X. Wang, Quantum Fisher information matrix and multiparameter estimation, J. Phys. A: Math. Theor. **53**, 023001 (2020).

[26] C. W. Helstrom, *Quantum Detection and Estimation Theory* (Academic, New York, 1976).

[27] A. S. Holevo, *Probabilistic and Statistical Aspects of Quantum Theory* (North-Holland, Amsterdam, 1982).

[28] S. L. Braunstein and C. M. Caves, Statistical Distance and the Geometry of Quantum States, Phys. Rev. Lett. **72**, 3439 (1994).

[29] D. Šafránek, Discontinuities of the quantum Fisher information and the Bures metric, Phys. Rev. A **95**, 052320 (2017).

[30] S. F. Huelga, C. Macchiavello, T. Pellizzari, A. K. Ekert, M. B. Plenio, and J. I. Cirac, Improvement of Frequency Standards with Quantum Entanglement, Phys. Rev. Lett. **79**, 3865 (1997).

[31] A. J. Leggett, S. Chakravarty, A. T. Dorsey, M. P. A. Fisher, A. Garg, and W. Zwerger, Dynamics of the dissipative two-state system, Rev. Mod. Phys. **59**, 1 (1987).

[32] R. Egger and C. H. Mak, Low-temperature dynamical simulation of spin-boson systems, Phys. Rev. B **50**, 15210 (1994).

[33] J. Eckel, J. H. Reina, and M. Thorwart, Coherent control of an effective two-level system in a non-Markovian biomolecular environment, New J. Phys. **11**, 085001 (2009).

[34] Y. Makhlin, G. Schön, and A. Shnirman, Quantum-state engineering with Josephson-junction devices, Rev. Mod. Phys. **73**, 357 (2001).

[35] M. Thorwart, J. Eckel, and E. R. Mucciolo, Non-Markovian dynamics of double quantum dot charge qubits due to acoustic phonons, Phys. Rev. B **72**, 235320 (2005).

[36] J. B. Yuan, H. J. Xing, L. M. Kuang, and S. Yi, Quantum non-Markovian reservoirs of atomic condensates engineered via dipolar interactions, Phys. Rev. A **95**, 033610 (2017).

[37] S. Blanes, F. Casas, J. A. Oteo, and J. Ros, The Magnus expansion and some of its applications, Phys. Rep. **470**, 151 (2009).

[38] N. Bar-Gill, D. D. Bhaktavatsala Rao, and G. Kurizki, Creating Nonclassical States of Bose-Einstein Condensates by Dephasing Collisions, Phys. Rev. Lett. **107**, 010404 (2011).

[39] Q. S. Tan, J. B. Yuan, G. R. Jin, and L. M. Kuang, Near-Heisenberg-limited parameter estimation precision by a dipolar-Bose-gas reservoir engineering, Phys. Rev. A **96**, 063614 (2017).

[40] Q. S. Tan, J. B. Yuan, J. Q. Liao, and L. M. Kuang, Supersensitive estimation of the coupling rate in cavity optomechanics with an impurity-doped Bose-Einstein condensate, Opt. Express **28**, 22867 (2020),

[41] A. W. Chin, S. F. Huelga, and M. B. Plenio, Quantum Metrology in Non-Markovian Environments, Phys. Rev. Lett. **109**, 233601 (2012)

[42] Y. J. Song, Q. S. Tan, and L. M. Kuang, Control quantum evolution speed of a single dephasing qubit for arbitrary initial states via periodic dynamical decoupling pulses, Sci. Rep. **7**, 43654 (2017).

[43] M. Napolitano, M. Koschorreck, B. Dubost *et al.*, Interaction-based quantum metrology showing scaling beyond the Heisenberg limit, Nature (London) **471**, 486 (2011).

[44] M. Zwierz, C. A. Pérez-Delgado, and P. Kok, General Optimality of the Heisenberg Limit for Quantum Metrology, Phys. Rev. Lett. **105**, 180402 (2010).

[45] M. J. W. Hall and H. M. Wiseman, Does Nonlinear Metrology Offer Improved Resolution? Answers from Quantum Information Theory, Phys. Rev. X **2**, 041006 (2012).

[46] G. R. Jin, Y. C. Liu, and W. M. Liu, Spin squeezing in a generalized one-axis twisting model, New J. Phys. **11**, 073049 (2009).